MATERIALS SCIENCE

Negative friction coefficient in microscale graphite/mica layered heterojunctions

Bingtong Liu[1,2], Jin Wang[3,4], Shuji Zhao[1,2,3], Cangyu Qu[3,4], Yuan Liu[1,2], Liran Ma[1,2], Zhihong Zhang[5], Kaihui Liu[5], Quanshui Zheng[1,3,4], Ming Ma[1,2,3]*

The friction of a solid contact typically shows a positive dependence on normal load according to classic friction laws. A few exceptions were recently observed for nanoscale single-asperity contacts. Here, we report the experimental observation of negative friction coefficient in microscale monocrystalline heterojunctions at different temperatures. The results for the interface between graphite and muscovite mica heterojunction demonstrate a robust negative friction coefficient both in loading and unloading processes. Molecular dynamics simulations reveal that the underlying mechanism is a synergetic and nontrivial redistribution of water molecules at the interface, leading to larger density and more ordered structure of the confined subnanometer-thick water film. Our results are expected to be applicable to other hydrophilic van der Waals heterojunctions.

INTRODUCTION

From the early tribological studies of Leonardo da Vinci to Amontons' law (*1*–*3*), the friction force F_f between two macroscopic bodies is believed to be proportional to the normal load F_N, that is, $F_f \sim \mu F_N$, where μ is the coefficient of friction (COF). Classic theories predict a positive COF, which means that the friction force increases with the increase of normal load due to the larger real contact area (*1*, *4*). This general trend has been confirmed by previous studies on various tribological systems (*5*, *6*). However, a few exceptions were observed recently, where counterintuitive examples were reported that the friction exhibited a complex dependence on normal load (*7*–*15*). In experiment, the friction of a nanoscale contact between an atomic force microscope (AFM) tip and chemically modified graphite or polymer-coated surfaces shows discrepancy for increasing (loading) and decreasing (unloading) normal loads (*14*, *15*). In the loading process, friction increases with normal load as common belief, while a negative friction coefficient (NFC) is found in the unloading process. This behavior is attributed to the strong adhesion between the tip and the specimen on substrates, which causes lifting and wrinkling of the top layers of specimen during tip retraction. Similar results are also found for tip on suspended graphene (*12*, *13*, *16*). In addition, a negative friction–load dependence is observed during the loading process for Si_3N_4 tip sliding on titanium substrate with ionic liquid–glycol ether mixtures in between as lubricant, which is resulted from the structural reorientation of the ionic liquid (*9*).

So far, the NFC phenomena reported experimentally can be only observed in either loading or unloading process on nanoscale. Obviously, this loading history dependence of NFC poses great challenges in its practical applications because one can only achieve NFC with either loading or unloading, which is usually not the case during actual operation out of the laboratory. The upscale of systems preserving NFC is another challenge as, up to now, the smallest commercial mechanical devices where friction plays a key role is on microscale, e.g., microelectromechanical systems (MEMS) (*17*, *18*). For such a market of US$ 18 billion for MEMS (*17*), the introduction of NFC as a distinct mechanical property would definitely bring new types of products.

Here, experimentally, we observe NFC for microscale graphite flake sliding on muscovite mica surface. The interface of the graphite/mica heterojunction is composed of two single-crystal surfaces, which enable a constant real contact area throughout the measurements. For both loading and unloading processes, the COF values are negative and on the order of 0.01. This shows that the NFC phenomenon is robust against loading history. The NFC is further observed with temperature ranging from room temperature (28°C) to 150°C. With extensive molecular dynamics (MD) simulations, we reveal that the underlying frictional mechanisms is a synergetic and nontrivial redistribution of water molecules at the interface, leading to the increased density and more ordered structure of the confined subnanometer-thick water film.

RESULTS

Graphite mesas (with typical size of 4 μm by 4 μm by 1 μm) with SiO_2 cap are fabricated according to previously developed procedures (see Materials and Methods for details) (*19*, *20*). In general, the mesas showing self-retraction motion (termed SRM mesas), i.e., the upper part of the mesa could self-retract to its initial position after being sheared with a tungsten tip and then releasing the tip, are identified. Then, the upper part of the graphite mesa, i.e., graphite flake, is transferred onto a freshly cleaved millimeter-sized muscovite mica to form microscale graphite/mica heterojunctions by using the technique developed in a previous work (*21*). With this procedure, the interface of the microscale graphite/mica heterojunction is composed of single-crystal surfaces.

Once fabricated, the graphite/mica heterojunction is annealed in dry nitrogen. Afterward, the heterojunction is manipulated by an AFM (NT-MDT, NTEGRA) equipped with an environment chamber. For friction test, the AFM tip (NT-MDT, VIT-P) is pressed onto the SiO_2 cap with a constant normal load to slide the graphite flake against the mica substrate at constant speed, as illustrated in Fig. 1A. No relative motion between the tip and the SiO_2 cap is observed. The sliding friction F_f of the heterojunction is estimated with a friction

[1]State Key Laboratory of Tribology, Tsinghua University, Beijing 100084, China. [2]Department of Mechanical Engineering, Tsinghua University, Beijing 100084, China. [3]Center for Nano and Micro Mechanics, Tsinghua University, Beijing 100084, China. [4]Department of Engineering Mechanics, Tsinghua University, Beijing 100084, China. [5]State Key Laboratory for Mesoscopic Physics, School of Physics, Peking University, Beijing 100871, China.
*Corresponding author. Email: maming16@tsinghua.edu.cn

loop, as shown in Fig. 1B. The dependence of friction on normal load F_N is investigated by changing F_N every 10 cycles and then calculating the mean value. The typical sliding displacement is 1 μm for both forward and backward scans, and the sliding velocity is 1 μm/s. The environmental chamber is filled with dry nitrogen throughout the measurement. More details about friction measurements can be found in Materials and Methods.

At room temperature (28°C) protected by N_2, unexpectedly, we observe NFC both in the loading and unloading processes, as shown in Fig. 1C. As the normal load increases by 104 μN, the friction drops notably from 3.4 to 1.8 μN. Fitting the F_f-F_N curves linearly yields the friction coefficient μ (defined as the slope of the curve) to be on the order of −0.01. Extended measurements with other 11 flakes of the same size yield similar results, as shown in Fig. 1D. For most of these flakes, the COFs in the loading and unloading regimes are both negative. Of 11 samples, only one exception is observed (flake #6), which is probably due to the wear of graphite flake. The presence of NFC both in loading and unloading processes is qualitatively different from the adhesion-induced NFC for nanoscale single-asperity contacts where NFC is only found in the unloading (*14*, *15*) or loading regime (*9*). In these systems (*14*), the F_f-F_N curve shows a hysteresis, i.e., at a given normal load during a load-unload cycle, the friction force measured during unloading is larger than that was measured while loading. Additional experiments are performed by changing the size and thickness of the graphite flake, and NFC is always observed, showing no dependence on the size and thickness (figs. S12 and S13).

The absence of hysteresis in the F_f-F_N curves in our experiments suggests that the observed NFC is not due to interface evolution during the sliding cycles. A validation is provided by the presence of NFC while changing the normal loads in random orders (fig. S2). This is further confirmed by fabricating a freshly graphite/mica heterojunction and subjecting it to 800 consequential sliding cycles under a constant normal load. The measured friction force slightly increases after a

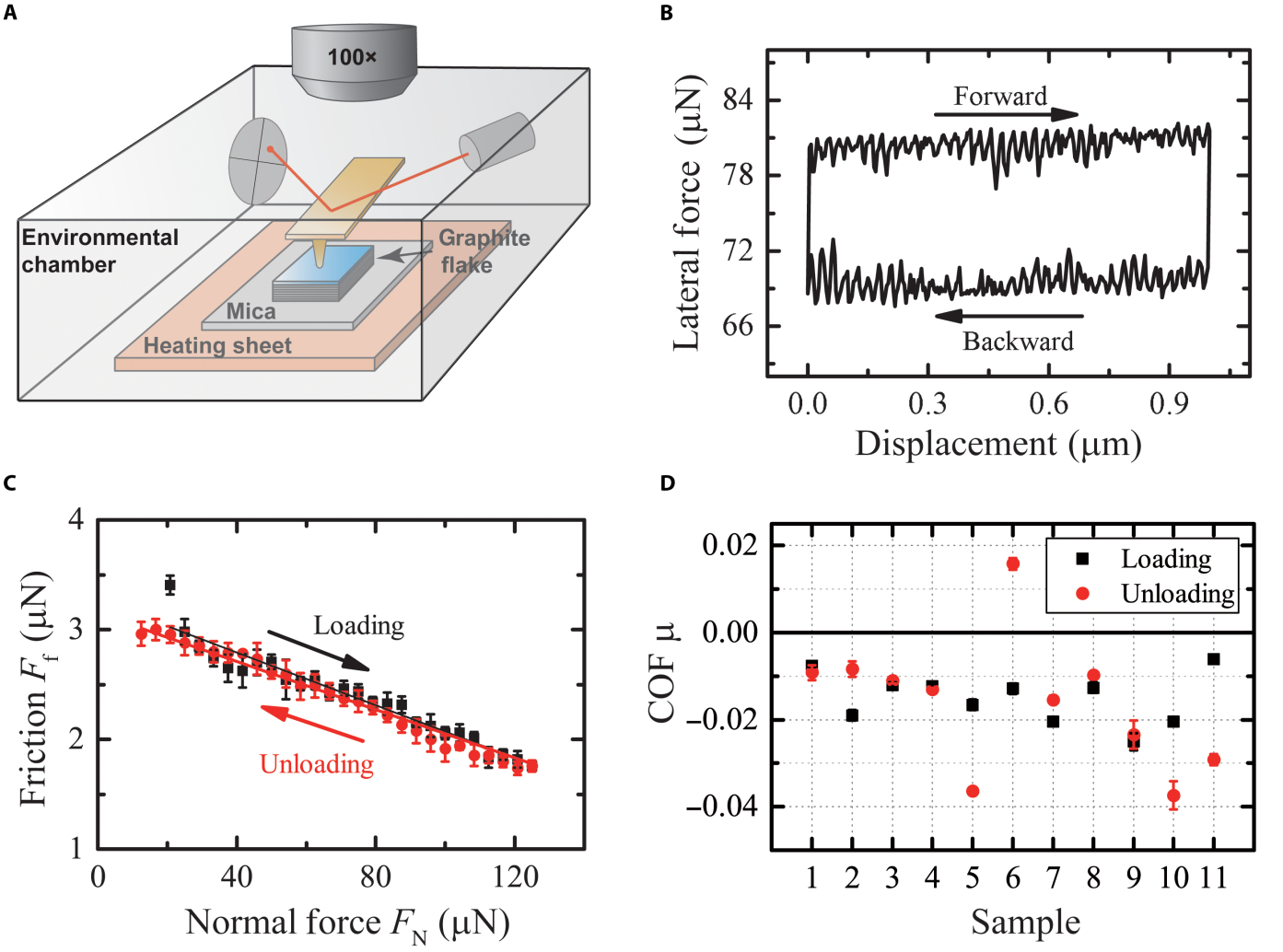

Fig. 1. NFC in graphite/mica heterojunctions. (**A**) Schematic diagram of the experimental setup. (**B**) A typical friction loop with the enclosed area being the energy dissipation ΔE for a displacement $D = 1$ μm. The friction is defined as $F_f = \Delta E/2D$. (**C**) The friction F_f shows a negative dependence on normal load F_N. The F_f-F_N curves in loading and unloading regimes almost overlap with each other. The slopes are defined as COF, which is found to be on the order of −0.01 (−0.012 ± 0.0005 for loading and −0.011 ± 0.0007 for unloading). (**D**) NFC is found in all the 11 flakes tested. The COF is found to be negative for both loading and unloading with only one exception (flake #6). The sliding velocity is 1 μm/s for all the tests.

"running-in" process. However, afterward, the friction still decreases as the normal load increases, showing NFC (fig. S3).

As temperature is an important factor governing friction (*22*, *23*), the normal load dependence of friction is measured at different temperatures ranging from room temperature (~28°C) to 150°C. NFC is observed at all temperatures, as shown in Fig. 2A. The results in Fig. 2B show that COF remains negative and almost constant for the same flake at temperature ranging from 28° to 150°C, suggesting that the observed NFC is robust against loading history under different temperatures. Meanwhile, the absolute value of friction force decreases with increasing temperature (Fig. 2C). Further measurements are conducted at different sliding velocities ranging from 0.1 to 10 μm/s. The friction is found to show a linear dependence on log(v), as shown in Fig. 2D. This velocity dependence, as well as the temperature dependence shown in Fig. 2C, is qualitatively consistent with the thermally activated Prandtl-Tomlinson model (*22*, *23*), suggesting that the friction phenomenon studied here is a rate process. The energy barrier is estimated to be on the order of 0.1 eV according to the Eyring model (*24*). After the friction measurement, the characterization results show that interfacial wear occurs on graphite/mica heterojunction (fig. S4). However, with careful investigation on the influence of wear on friction force, we find that the wear debris always increases friction. Thus, interfacial wear is not the cause of NFC (fig. S6).

For the influence of environment, with similar systems (graphite/*h*-BN), previous study (*5*) shows that, besides temperature, the humidity could also affect friction. To this end, we measure the friction of another set of samples prepared by exposing the mica surface to N_2 with a relative humidity (RH) of ~60% before transferring the graphite flake onto the mica surface. Subsequent friction measurements are conducted under ambient conditions (RH, ~22%; temperature, ~28°C) without annealing. Because of the exposure to humid environment before transfer process, water films are expected to grow at the graphite/mica interface (*25*). As shown in Fig. 3, contradictory to the NFC results described above, for all the samples, we observe a positive COF in the loading regime and a negative COF in the unloading regime (Fig. 3A), which shows hysteresis in friction. For the same sample, three consecutive loading-unloading tests are

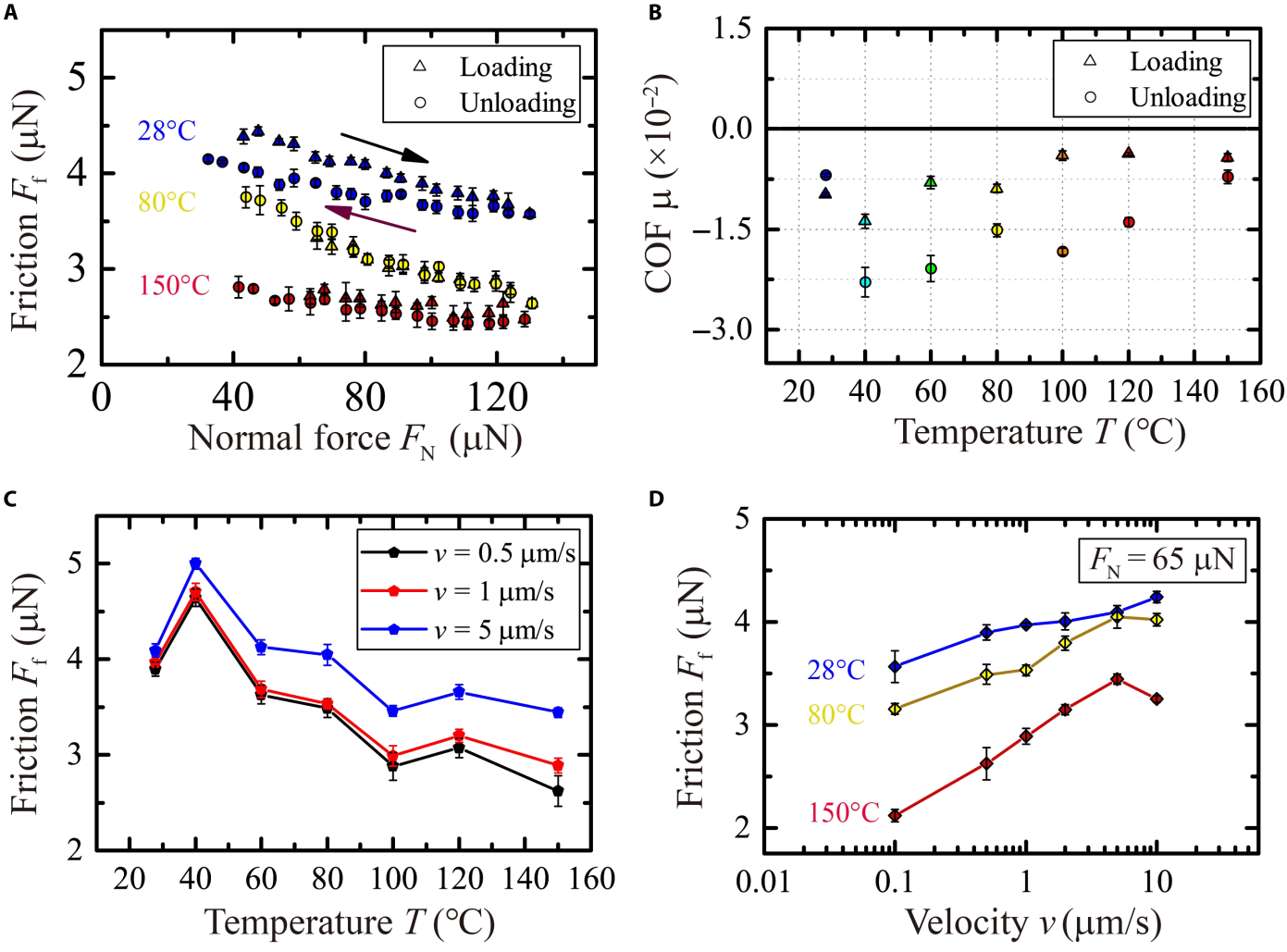

Fig. 2. NFC at different temperatures and velocities measured experimentally. (**A**) NFC is found for the same flake at temperature ranging from room temperature (28°C) to 150°C. (**B**) COF as a function of temperature. NFC is found for all the temperatures tested. (**C**) Friction force under a normal load of 65 μN as a function of temperature (sliding velocity is 0.5, 1, and 5 μm/s, respectively). (**D**) Friction force under a normal load of 65 μN as a function of sliding velocity (temperature, 28°, 80°, and 150°C). All the error bars in these figures are calculated as the SDs of five independent friction loops.

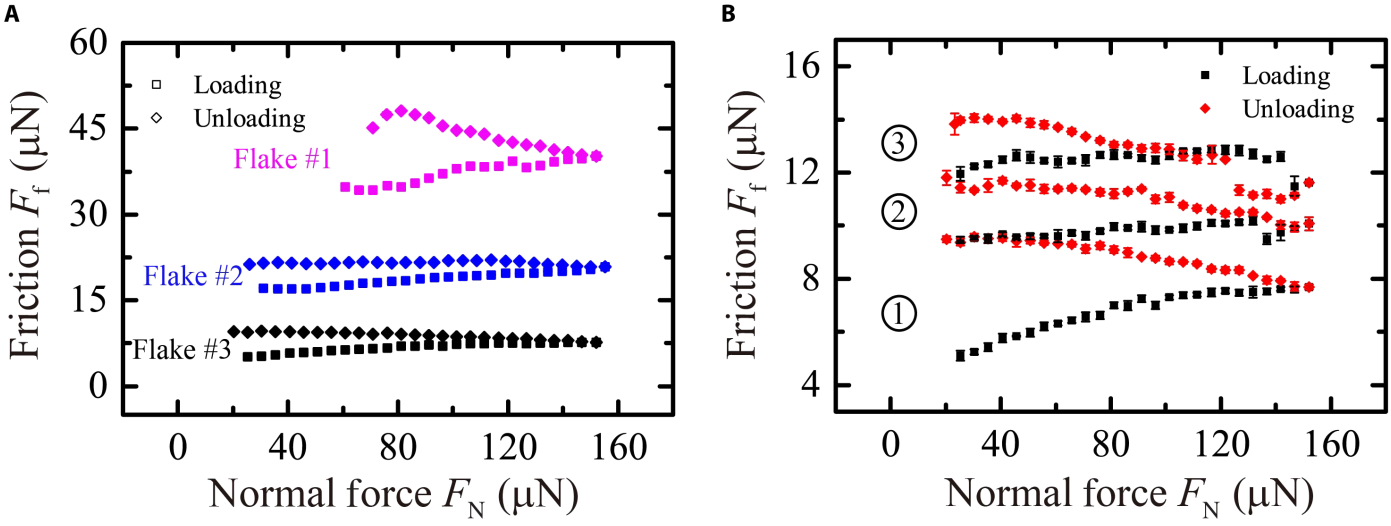

Fig. 3. Friction measured experimentally for the graphite/mica heterojunction treated with RH ~60%. (**A**) The friction dependence on normal load for three samples. The slope from bottom to top is 0.020, −0.011; 0.031, 0.006; and 0.065, −0.112, respectively. (**B**) Friction of three consecutive measurements for the same sample. The slope from bottom to top is 0.020, −0.011; 0.005, −0.012; and 0.005, −0.018, respectively. The typical fitting error for the slope is 8.55×10^{-4}. The error bars for all the data points are too small to be observed. A typical error bar for F_f is 0.153 μN. The sliding displacement is 1 μm, and the sliding velocity is 1 μm/s. The results are measured under ambient conditions (RH of ~22%) at room temperature (~28°C) after treated in high humidity.

performed (Fig. 3B). The friction measured suggests that the hysteresis is due to the continuous increase of friction as sliding process proceeds. In other words, the friction increases with sliding cycles regardless of normal load. Thus, during the unloading process, the normal load decreases, and friction increases with sliding cycles, leading to an apparent NFC. Characterizations of the sliding interface suggest that such an evolution effect is due to severe wear of the interface in high humidity (fig. S5).

The effect of humidity is further examined for the same heterojunction, where the load-dependent friction is first measured after annealing and then measured again after being treated in high humidity. Similar to Fig. 1C, a clear NFC phenomenon is observed both in loading and unloading processes before humidifying. For the same samples measured after further humidifying, however, NFC only appears in unloading process. Because the same sample is measured for different humidity, we find that friction increases greatly when humidity increases from RH of ~5% to RH of ~60%, which indicates the increase in the amount of water leading to larger friction (fig. S7).

DISCUSSION

To understand the NFC in graphite/mica heterojunctions annealed under dry nitrogen, we first consider several possible mechanisms reported in literatures. The adhesion-induced NFC is due to the lifting and wrinkling of top materials on substrates during tip retraction (*14*, *15*) and thus only emerges in the unloading regime, which is not consistent with our results where NFC is observed both in loading and unloading processes. Meanwhile, pressure-induced flattening of potential energy surface corrugation can result in NFC for both loading and unloading processes according to theoretical predictions (*8*, *10*, *26*). However, the pressure needed to induce this effect is on the order of 100 GPa, which is three orders of magnitude higher than the maximum pressure of 0.75 GPa in our experiments (fig. S8). Very recently, NFC is found in superlubric graphite/*h*-BN heterojunctions using MD simulations. It originates from the load-induced suppression of the out-of-plane distortions in Moiré superstructure, leading to a less dissipative interfacial dynamics (*7*). However, in this case, the friction increases as temperature increases, which is qualitatively different from our experimental observations showing negative dependence. Another possibility for the cause of NFC under nitrogen atmosphere would be the variation of real contact upon loading/unloading. This mechanism is also excluded because our finite-element analysis for the microscale contact shows that the real contact area remains unchanged (fig. S8), which is understandable by considering the large adhesion between the surfaces.

By examining the experimental phenomena carefully, we notice that an important clue for revealing the underlying mechanism is the presence of water. For the heterojunctions treated in high RH environment, the friction exhibits hysteresis, and no negative dependence is observed. It is well known that under ambient conditions, freshly cleaved mica substrate is hydrophilic and will inevitably absorb a heterogeneous water film (whole layer or islands of water molecules) with a thickness depending on the ambient RH (*25*, *27*, *28*). For the coverage of water film confined between mica and graphene, experimentally, Song *et al.* (*29*) found that even heating the sample at 100°C for half an hour, the water film still exists with a coverage of 70%. Our characterization of confined water between graphene and mica by sum frequency generation (SFG) spectroscopy and AFM show that water layer exactly exists at the graphene/mica interface (figs. S14 and S15).

To explore the influence of water film on the counterintuitive friction behavior, we perform MD simulations with details shown in Materials and methods. Throughout the simulation, water molecules are stuck to the mica surface due to the strong coulombic interaction and form hydration shells around the potassium ion (Fig. 4A). Thus, no Moiré pattern is formed. The simulation results show a similar NFC behavior on the order of −0.01 as found in our experiments. The out-of-plane deformation of the lowest graphene layer $h = \langle \Delta z^2 \rangle^{1/2}$ decreases with the increase of normal force F_N as shown in

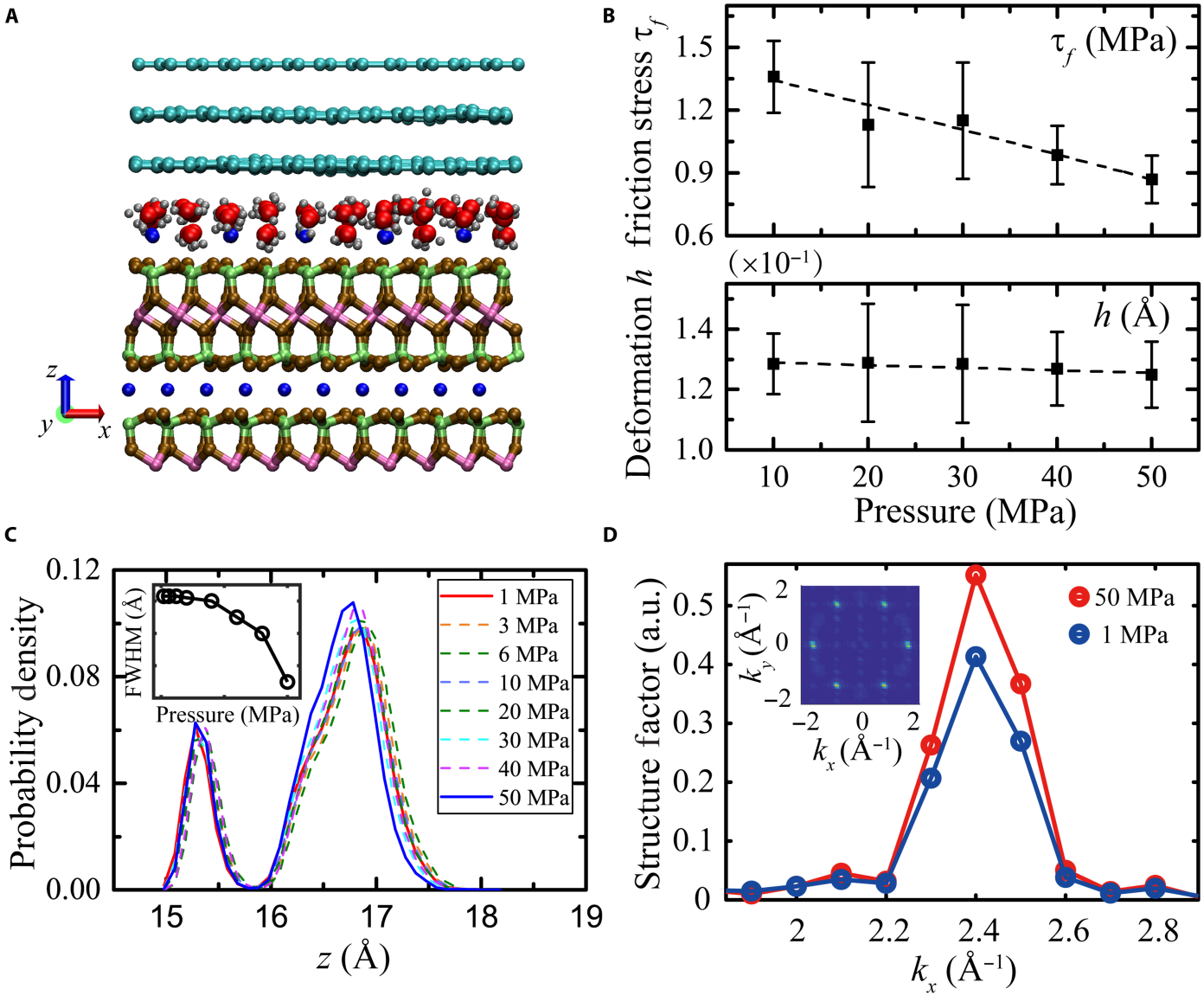

Fig. 4. MD simulation results of NFC. (**A**) The simulation model of the graphite/mica heterojunction. From the top to bottom, the atoms in cyan, red, gray, blue, brown, green, and pink are carbon, oxygen in water, hydrogen, potassium, oxygen in mica, silicon, and aluminum, respectively. (**B**) Relationship between the friction stress τ_f (top) and out-of-plane deformation h (bottom) of the bottom graphene layer and the normal load pressure. The dashed lines are the linear fitting of the data points. The COF fitted is −0.012 ± 0.001. (**C**) Probability density distribution of oxygen atoms in water molecules along z axis. Full width at half maximum (FWHM) of the oxygen atom under different normal pressure is shown in the inset. (**D**) Structure factor of the oxygen atoms in water molecules along $\vec{k}_x$ direction, while inset shows the two-dimensional landscape of the structure factor. a.u., arbitrary units.

Fig. 4B (fig. S9), resulting in a smoother surface. This reduced out-of-plane deformation upon loading is analogous to a recently reported mechanism for NFC observed for graphite/*h*-BN heterojunction with Moiré patterns via MD simulation, however, without water molecules. Since the sliding occurs at the water/graphene interface as observed in our simulation, it is intuitive to assume that the friction will decrease correspondingly because of the smoother interface.

The phenomenological mechanism is further investigated by calculating the structural change of water film as normal load varies. As shown in Fig. 4C, the full width at half maximum of the probability density distribution of oxygen atoms in water molecules along the z axis decreases as F_N increases. Meanwhile, the thickness of water film also decreases slightly. The sixfold structure factor of oxygen atoms in water as shown in the inset of Fig. 4D indicates a solid-like structure of the water film. As F_N increases, the peak value of structure factor increases, indicating that the structure of water film becomes more ordered. Because of the mismatch between the graphene lattice ($k \sim 2.554$) and the solid-like water lattice ($k \sim 2.4$), the NFC found in our simulation is potentially assisted by structural lubricity (*5*). The simultaneous structural changes of water film perpendicular and parallel to the solid surfaces indicate a synergetic and nontrivial redistribution of water molecules, leading to the increased density and the more ordered structure of the water film confined, and lastly account for a smoother sliding interface, causing

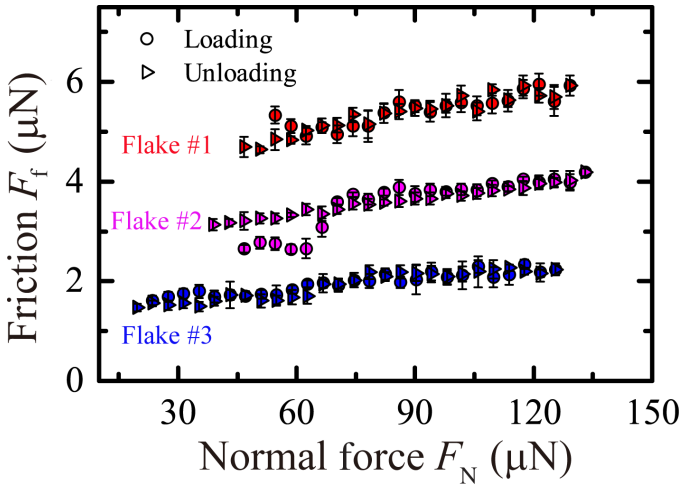

Fig. 5. Load-dependent friction for the graphite/WSe_2 heterojunctions measured experimentally. The COF for flake #1, flake #2, and flake #3 is 0.0067 (loading), 0.0083 (unloading); 0.0074 (loading), 0.0101 (unloading); and 0.0118 (loading), 0.0165 (unloading). The typical fitting error for COF is 4.57×10^{-4}. The sliding displacement is 1 μm, and the sliding velocity is 1 μm/s. The results are measured in dry nitrogen (RH of <5%) at room temperature (~28°C).

the friction collapses under higher normal loads. In light of these discoveries, a simulation without water film confined between graphite and mica at 298 K is conducted. For such a system, no NFC is observed (fig. S10), confirming that the water film does play an important role.

From above simulations, the water film is indispensable to observe NFC for graphite/mica heterojunction. This essential role of the water film is verified by performing another frictional experiment for graphite/WSe_2 heterojunction. The structure of WSe_2 is of hexagonal MoS_2 structure type. Its contact angle for water droplets is more than 100° (*30*), providing a much more hydrophobic surface compared with freshly cleaved mica with contact angle being 0°. Further SFG spectroscopy characterization shows no water presents on the WSe_2 substrate (fig. S16). The microscale graphite/WSe_2 heterojunction is prepared with the same fabrication process. Then, the heterojunctions are annealed in dry nitrogen (RH of <5%) for an hour and recover to room temperature. The load-dependent friction is measured in dry nitrogen (RH of <5%) at room temperature (~28°C). Different from the results obtained for graphite/mica heterojunctions, the friction here shows a positive dependence on the normal load for both loading and unloading processes, as shown in Fig. 5. The COF for graphite/WSe_2 system is between 0.007 and 0.017. No wear occurs after the measurement (fig. S11). The positive friction coefficient for graphite/WSe_2 demonstrates that the water film is critical to observe NFC in graphite/mica systems, validating the mechanisms revealed via MD simulations.

In summary, NFC is observed in microscale monocrystalline graphite/mica heterojunctions after annealing. The NFC phenomenon is robust against loading history at different temperatures. MD simulations reveal that a synergetic and nontrivial redistribution of water molecules leading to the increased density and more ordered structure of the confined water film is responsible for NFC. The mechanism is validated with a comparative experiment using microscale graphite/WSe_2 heterojunctions. Our results may provide a viable approach to achieve ultralow friction for van der Waals heterojunctions, which has a potential impact on a broad range of engineering applications such as MEMS. The mechanism revealed also brings previously unknown understanding for the frictional phenomenon on microscale, especially for van der Waals heterojunctions.

MATERIALS AND METHODS

Preparation of graphite/mica heterojunction

The microfabrication techniques are similar to those reported in (*31*) and in our previous articles (*19*, *20*, *32*, *33*). Specifically, graphite flakes (with a typical size of 4 μm by 4 μm by 1 μm) capped with a 200-nm-thick SiO_2 film on the top are fabricated. Then, the graphite flakes exhibiting SRM (termed SRM graphite flake) (*19*, *20*) are selected. The graphite/mica heterojunctions are fabricated by transferring the SRM graphite flake onto the millimeter-sized muscovite mica freshly air-cleaved under ambient conditions. By such a direct transfer method, a monocrystalline graphite/mica heterojunction can be fabricated, the interface of which has been confirmed to be flat and clean with the height fluctuations less than 1 nm (*21*). The process of the sample preparation is carried out under ambient conditions at a room temperature of 28°C and RH of 22%.

Once fabricated, the assembled graphite/mica heterojunction is manipulated by a commercial AFM equipped with a 100× objective lens. A closed chamber is used to measure the friction dependence on normal load in various environments. Two different sample treatment methods are involved. Method 1: The entire fabricated graphite/mica heterojunctions are held for 1 hour at a temperature of 150°C under nitrogen atmosphere (RH of <5%) and then cooled to the room temperature (~28°C), which is called annealing under nitrogen atmosphere. Subsequent friction measurements are all conducted under nitrogen atmosphere with the temperature ranging from room temperature to 150°C randomly. Method 2: The second environment for graphite/mica heterojunctions has different fabrication process from the above samples. The air-cleaved bare mica is first held for 1 hour in the nitrogen atmosphere with an RH of 60%, which enables the complete water films to grow on mica (*25*, *28*). Then, a transfer process of graphite flake and subsequent friction measurements are performed under ambient conditions. In this case, the amount of water confined at the interface is larger than that fabricated with method 1. The friction is measured under ambient conditions.

AFM tests

As illustrated in Fig. 1A, the experimental setup is composed of a commercial AFM (NT-MDT, NTEGRA), a 100-μm piezoelectric scanning tube, a 100× objective lens with an aperture of 0.7 (Mitutoyu), a heating stage (NT-MDT, SU045NTF) with temperature ranging from room temperature to 150°C, and an environmental chamber. During the measurement process, a top visual tip (VIT-P/IR; nominal spring constant, 50 N/m) is used to press the SiO_2 cap on the top of the graphite flake and slide the flake laterally relative to the mica substrate at a constant speed. For all the heterojunctions, the friction is measured as normal load increases first and then decreases, which is called loading and unloading processes, respectively. Limited to the spring constant of AFM tip, the range of the normal load is about 20 to 150 μN. The typical sliding displacement is 1 μm, and the sliding velocity is 1 μm/s. The friction dependence on sliding velocity is also measured under nitrogen atmosphere with a range of 0.1 to 10 μm/s. All the experiments are operated under one-line

mode, i.e., the AFM tip is always conducted reciprocating motion along the same line. A standard calibration method is adopted for both normal (*34*, *35*) and friction (*36*) forces (fig. S1). After annealing, the friction is measured at room temperature (~28°C) under nitrogen atmosphere (RH of <5%).

MD simulation

The model consists of one mica substrate with the formula of $KAl_2(AlSi_3)O_{10}$, water molecules, and graphene slider (Fig. 4A). The bottom and middle graphene layers are flexible, while the top graphene layer is rigid. According to our previous work (*5*), friction contributed from rim area is negligible in this system; thus, periodic boundary condition is used in our simulations with lengths in the x and y directions of 25.99 and 27.08 Å, respectively. Fifteen potassium ions remain on the mica surface so that the simulated system is electrically neutral. Given that mica is hydrophilic, water molecules are introduced to this model system regardless of the annealing treatment (*29*). The model with 75 molecules was used to qualitatively mimic the low humidity environment in experiments.

The MD simulations are performed using Large-scale Atomic/Molecular Massively Parallel Simulator (LAMMPS) (*37*). The interaction between the mica and graphene flake is described by ClayFF (*38*), and graphene flake is described by the Lennard-Jones (LJ) potential with $\varepsilon = 0.07$ kcal/mol and $\sigma = 3.55$ Å (*39*). The interaction between graphene layers is calculated by the Kolmogorov-Crespi potential (*40*). The intralayer interaction of graphene layers is computed by the REBO force field (*41*). Water is modeled using rigid SPC/E (Extended Simple Point Charge) (*42*). Bond lengths and angles in water molecules are constrained using the SHAKE algorithm (*43*). All the cross-term LJ interactions are estimated using the Lorentz-Berthelot mixing rules. The LJ potential and electrostatic interactions are both truncated at a distance of 12 Å. Long-range electrostatic interactions are calculated with the particle-particle particle-mesh (PPPM) method (*44*).

All simulations are conducted at room temperature $T = 298$ K with Nose-Hoover thermostat to the middle graphene layer. A spring with stiffness $K_s = 10$ N/m (*45*) moving at a speed of $V_0 = 10$ m/s is attached to the upper layer of graphene. The pressure is introduced by applying normal force to each atom in the upper graphene. A fixed time step of 1 fs is used. Along y direction, springs are added to each carbon atom within the upper layer of the graphite flake with spring constant $k = K_s/N_{up}$ to stand for the constraint exerted by the tip, where N_{up} is the total number of atoms of the upper flake. The sliding friction is calculated as $\langle F_s \rangle = \langle K_s (V_0 t - X_{com}) \rangle$, where X_{com} is the center of mass of the upper graphene and $\langle \cdot \rangle$ denoted an ensemble average over the steady states. For each simulation, we first perform the energy minimization and then equilibrate the system for 500 ps. After that, a further 10-ns simulation is performed to collect data.

SUPPLEMENTARY MATERIALS

Supplementary material for this article is available at http://advances.sciencemag.org/cgi/content/full/6/16/eaaz6787/DC1

REFERENCES AND NOTES

1. J. Gao, W. D. Luedtke, D. Gourdon, M. Ruths, J. N. Israelachvili, U. Landman, Frictional forces and Amontons' law: From the molecular to the macroscopic scale. *J. Phys. Chem. B* **108**, 3410–3425 (2004).
2. A. Berman, C. Drummond, J. Israelachvili, Amontons' law at the molecular level. *Tribol. Lett.* **4**, 95–101 (1998).
3. Z. Chen, A. Khajeh, A. Martini, S. H. Kim, Chemical and physical origins of friction on surfaces with atomic steps. *Sci. Adv.* **5**, eaaw0513 (2019).
4. H. Sakuma, K. Kawai, I. Katayama, S. Suehara, What is the origin of macroscopic friction? *Sci. Adv.* **4**, eaav2268 (2018).
5. Y. Song, D. Mandelli, O. Hod, M. Urbakh, M. Ma, Q. Zheng, Robust microscale superlubricity in graphite/hexagonal boron nitride layered heterojunctions. *Nat. Mater.* **17**, 894–899 (2018).
6. S.-W. Liu, H.-P. Wang, Q. Xu, T.-B. Ma, G. Yu, C. Zhang, D. Geng, Z. Yu, S. Zhang, W. Wang, Y.-Z. Hu, H. Wang, J. Luo, Robust microscale superlubricity under high contact pressure enabled by graphene-coated microsphere. *Nat. Commun.* **8**, 14029 (2017).
7. D. Mandelli, W. Ouyang, O. Hod, M. Urbakh, Negative friction coefficients in superlubric graphite–hexagonal boron nitride heterojunctions. *Phys. Rev. Lett.* **122**, 076102 (2019).
8. J. Sun, Y. Zhang, Z. Lu, Q. Li, Q. Xue, S. Du, J. Pu, L. Wang, Superlubricity enabled by pressure-induced friction collapse. *J. Phys. Chem. Lett.* **9**, 2554–2559 (2018).
9. R. An, G. Zhou, Y. Zhu, W. Zhu, L. Huang, F. U. Shah, Friction of ionic liquid–glycol ether mixtures at titanium interfaces: Negative load dependence. *Adv. Mater. Interfaces* **5**, 1800263 (2018).
10. J. Sun, Y. Zhang, Z. Lu, Q. Xue, L. Wang, Attraction induced frictionless sliding of rare gas monolayer on metallic surfaces: An efficient strategy for superlubricity. *Phys. Chem. Chem. Phys.* **19**, 11026–11031 (2017).
11. J. Chen, W. Gao, Unconventional behavior of friction at the nanoscale beyond Amontons' law. *ChemPhysChem* **18**, 2033–2039 (2017).
12. Z. Ye, A. Martini, Atomistic simulation of the load dependence of nanoscale friction on suspended and supported graphene. *Langmuir* **30**, 14707–14711 (2014).
13. A. Smolyanitsky, J. P. Killgore, Anomalous friction in suspended graphene. *Phys. Rev. B* **86**, 125432 (2012).
14. Z. Deng, A. Smolyanitsky, Q. Li, X.-Q. Feng, R. J. Cannara, Adhesion-dependent negative friction coefficient on chemically modified graphite at the nanoscale. *Nat. Mater.* **11**, 1032–1037 (2012).
15. E. Thormann, Negative friction coefficients. *Nat. Mater.* **12**, 468 (2013).
16. Z. Deng, N. N. Klimov, S. D. Solares, T. Li, H. Xu, R. J. Cannara, Nanoscale interfacial friction and adhesion on supported versus suspended monolayer and multilayer graphene. *Langmuir* **29**, 235–243 (2012).
17. J. G. Vilhena, R. Pérez, Slippery in every direction. *Nat. Mater.* **17**, 852–854 (2018).
18. O. Hod, E. Meyer, Q. Zheng, M. Urbakh, Structural superlubricity and ultralow friction across the length scales. *Nature* **563**, 485–492 (2018).
19. Z. Liu, J. Yang, F. Grey, J. Z. Liu, Y. Liu, Y. Wang, Y. Yang, Y. Cheng, Q. Zheng, Observation of microscale superlubricity in graphite. *Phys. Rev. Lett.* **108**, 205503 (2012).
20. Q. Zheng, B. Jiang, S. Liu, Y. Weng, L. Lu, Q. Xue, J. Zhu, Q. Jiang, S. Wang, L. Peng, Self-retracting motion of graphite microflakes. *Phys. Rev. Lett.* **100**, 067205 (2008).
21. B. Liu, J. Wang, X. Peng, C. Qu, M. Ma, Q. Zheng, Direct fabrication of graphite-mica heterojunction and in situ control of their relative orientation. *Mater. Design* **160**, 371–376 (2018).
22. Y. Sang, M. Dubé, M. Grant, Thermal effects on atomic friction. *Phys. Rev. Lett.* **87**, 174301 (2001).
23. A. Vanossi, N. Manini, M. Urbakh, S. Zapperi, E. Tosatti, Modeling friction: From nanoscale to mesoscale. *Rev. Mod. Phys.* **85**, 529–552 (2013).
24. T. Bouhacina, J. P. Aimé, S. Gauthier, D. Michel, V. Heroguez, Tribological behavior of a polymer grafted on silanized silica probed with a nanotip. *Phys. Rev. B* **56**, 7694–7703 (1997).
25. A. Schumacher, N. Kruse, R. Prins, E. Meyer, R. Lüthi, L. Howald, H.-J. Güntherodt, L. Scandella, Influence of humidity on friction measurements of supported MoS_2 single layers. *J. Vac. Sci. Technol. B* **14**, 1264–1267 (1996).
26. M. C. Righi, M. Ferrario, Pressure induced friction collapse of rare gas boundary layers sliding over metal surfaces. *Phys. Rev. Lett.* **99**, 176101 (2007).
27. N. Severin, P. Lange, I. M. Sokolov, J. P. Rabe, Reversible dewetting of a molecularly thin fluid water film in a soft graphene–mica slit pore. *Nano Lett.* **12**, 774–779 (2012).
28. J. Hu, X.-D. Xiao, D. F. Ogletree, M. Salmeron, Imaging the condensation and evaporation of molecularly thin films of water with nanometer resolution. *Science* **268**, 267–269 (1995).
29. J. Song, Q. Li, X. Wang, J. Li, S. Zhang, J. Kjems, F. Besenbacher, M. Dong, Evidence of Stranski–Krastanov growth at the initial stage of atmospheric water condensation. *Nat. Commun.* **5**, 4837 (2014).
30. N. D. Boscher, C. J. Carmalt, I. P. Parkin, Atmospheric pressure chemical vapor deposition of WSe_2 thin films on glass—Highly hydrophobic sticky surfaces. *J. Mater. Chem.* **16**, 122–127 (2006).
31. X. Lu, M. Yu, H. Huang, R. S. Ruoff, Tailoring graphite with the goal of achieving single sheets. *Nanotechnology* **10**, 269–272 (1999).
32. J. Yang, Z. Liu, F. Grey, Z. Xu, X. Li, Y. Liu, M. Urbakh, Y. Cheng, Q. Zheng, Observation of high-speed microscale superlubricity in graphite. *Phys. Rev. Lett.* **110**, 255504 (2013).

33. W. Wang, S. Dai, X. Li, J. Yang, D. J. Srolovitz, Q. Zheng, Measurement of the cleavage energy of graphite. *Nat. Commun.* **6**, 7853 (2015).
34. J. E. Sader, J. W. M. Chon, P. Mulvaney, Calibration of rectangular atomic force microscope cantilevers. *Rev. Sci. Instrum.* **70**, 3967–3969 (1999).
35. J. E. Sader, I. Larson, P. Mulvaney, L. R. White, Method for the calibration of atomic force microscope cantilevers. *Rev. Sci. Instrum.* **66**, 3789–3798 (1995).
36. D. F. Ogletree, R. W. Carpick, M. Salmeron, Calibration of frictional forces in atomic force microscopy. *Rev. Sci. Instrum.* **67**, 3298–3306 (1996).
37. S. Plimpton, Fast parallel algorithms for short-range molecular dynamics. *J. Comput. Phys.* **117**, 1–19 (1995).
38. E. S. Boek, P. V. Coveney, N. T. Skipper, Monte Carlo molecular modeling studies of hydrated Li-, Na-, and K-smectites: Understanding the role of potassium as a clay swelling inhibitor. *J. Am. Chem. Soc.* **117**, 12608–12617 (1995).
39. R. C. Sinclair, J. L. Suter, P. V. Coveney, Graphene–graphene interactions: Friction, superlubricity, and exfoliation. *Adv. Mater.* **30**, e1705791 (2018).
40. A. N. Kolmogorov, V. H. Crespi, Registry-dependent interlayer potential for graphitic systems. *Phys. Rev. B* **71**, 235415 (2005).
41. D. W. Brenner, O. A. Shenderova, J. A. Harrison, S. J. Stuart, B. Ni, S. B. Sinnott, A second-generation reactive empirical bond order (REBO) potential energy expression for hydrocarbons. *J. Phys. Condens. Matter.* **14**, 783–802 (2002).
42. H. J. C. Berendsen, J. R. Grigera, T. P. Straatsma, The missing term in effective pair potentials. *J. Phys. Chem.* **91**, 6269–6271 (1987).
43. J.-P. Ryckaert, G. Ciccotti, H. J. C. Berendsen, Numerical integration of the cartesian equations of motion of a system with constraints: Molecular dynamics of n-alkanes. *J. Comput. Phys.* **23**, 327–341 (1977).
44. T. Darden, D. York, L. Pedersen, Particle mesh Ewald: An N·log(N) method for ewald sums in large systems. *J. Chem. Phys.* **98**, 10089–10092 (1993).
45. W. Ouyang, D. Mandelli, M. Urbakh, O. Hod, Nanoserpents: Graphene nanoribbon motion on two-dimensional hexagonal materials. *Nano Lett.* **8**, 6009–6016 (2018).
46. L.-F. Wang, Q.-S. Zheng, Extreme anisotropy of graphite and single-walled carbon nanotube bundles. *Appl. Phys. Lett.* **90**, 153113 (2007).
47. J. Li, J. Li, J. Luo, Superlubricity of graphite sliding against graphene nanoflake under ultrahigh contact pressure. *Adv. Sci.* **5**, 1800810 (2018).
48. J. Li, T. Gao, J. Luo, Superlubricity of graphite induced by multiple transferred graphene nanoflakes. *Adv. Sci.* **5**, 1700616 (2017).
49. S. Wang, Y. Zhang, N. Abidi, L. Cabrales, Wettability and surface free energy of graphene films. *Langmuir* **25**, 11078–11081 (2009).
50. H. K. Christenson, Adhesion and surface energy of mica in air and water. *J. Phys. Chem.* **97**, 12034–12041 (1993).
51. L. Bergström, Hamaker constants of inorganic materials. *Adv. Colloid Interface Sci.* **70**, 125–169 (1997).
52. G. De Falco, M. Commodo, P. Minutolo, A. D'Anna, Flame-formed carbon nanoparticles: Morphology, interaction forces, and hamaker constant from AFM. *Aerosol Sci. Tech.* **49**, 281–289 (2015).
53. K. Xu, P. Cao, J. R. Heath, Graphene visualizes the first water adlayers on mica at ambient conditions. *Science* **329**, 1188–1191 (2010).
54. X. Xu, Z. Zhang, J. Dong, D. Yi, J. Niu, M. Wu, L. Lin, R. Yin, M. Li, J. Zhou, S. Wang, J. Sun, X. Duan, P. Gao, Y. Jiang, X. Wu, H. Peng, R. S. Ruoff, Z. Liu, D. Yu, E. Wang, F. Ding, K. Liu, Ultrafast epitaxial growth of metre-sized single-crystal graphene on industrial Cu foil. *Sci. Bull.* **62**, 1074–1080 (2017).
55. O. Ochedowski, B. Kleine Bussmann, M. Schleberger, Graphene on Mica - intercalated water trapped for life. *Sci. Rep.* **4**, 6003 (2015).
56. K. T. He, J. D. Wood, G. P. Doidge, E. Pop, J. W. Lyding, Scanning tunneling microscopy study and nanomanipulation of graphene-coated water on Mica. *Nano Lett.* **12**, 2665–2672 (2012).
57. Q. Li, C. Lee, R. W. Carpick, J. Hone, Substrate effect on thickness-dependent friction on graphene. *Phys. Status Solidi B* **247**, 2909–2914 (2010).
58. Q. Du, E. Freysz, Y. R. Shen, Vibrational spectra of water molecules at quartz/water interfaces. *Phys. Rev. Lett.* **72**, 238–241 (1994).
59. Q. Du, R. Superfine, E. Freysz, Y. R. Shen, Vibrational spectroscopy of water at the vapor/water interface. *Phys. Rev. Lett.* **70**, 2313–2316 (1993).

Acknowledgments

Funding: This work was supported by the National Natural Science Foundation of China (grant nos. 11890673, 11772168, and 11890671). **Author contributions:** M.M. and B.L. conceived the original idea. M.M. supervised the research project. B.L. conducted the frictional and characterization experiments. J.W. carried out the MD simulations. S.Z. performed the finite-element analysis. Y.L. and L.M. performed the SFG spectroscopy measurement. Z.Z. and K.L. provided the sample of graphene coated on mica. B.L., J.W., C.Q., and M.M. interpreted the experimental results and simulation data. All authors contributed to the writing of the manuscript. **Competing interests:** The authors declare that they have no competing interests. **Data and materials availability:** All data needed to evaluate the conclusions in the paper are present in the paper and/or the Supplementary Materials. Additional data related to this paper may be requested from the authors.

Submitted 30 September 2019
Accepted 22 January 2020
Published 17 April 2020
10.1126/sciadv.aaz6787

Citation: B. Liu, J. Wang, S. Zhao, C. Qu, Y. Liu, L. Ma, Z. Zhang, K. Liu, Q. Zheng, M. Ma, Negative friction coefficient in microscale graphite/mica layered heterojunctions. *Sci. Adv.* **6**, eaaz6787 (2020).

Negative friction coefficient in microscale graphite/mica layered heterojunctions

Bingtong Liu, Jin Wang, Shuji Zhao, Cangyu Qu, Yuan Liu, Liran Ma, Zhihong Zhang, Kaihui Liu, Quanshui Zheng and Ming Ma

Sci Adv **6** (16), eaaz6787.
DOI: 10.1126/sciadv.aaz6787